Advances in Science and Technology Research Journal

Advances in Science and Technology Research Journal 2023, 17(2), 36–52
https://doi.org/10.12913/22998624/159723
ISSN 2299–8624, License CC-BY 4.0

Received: 2022.12.30
Accepted: 2023.03.01
Published: 2023.04.01

Numerical Modelling and Experimental Testing on Polyurethane Adhesively Bonded Joints Behaviour in Wood-Wood and Wood-Carbon Fibre Reinforced Polymer Layouts

Bartosz Kawecki[1*]

[1] Faculty of Civil Engineering and Architecture, Lublin University of Technology, ul. Nadbystrzycka 40, 20-618 Lublin, Poland

* Corresponding author's e-mail: b.kawecki@pollub.pl

ABSTRACT

Scientists do a variety of laboratory tests on timber and wood-containing composites. An example is adhesively bonded joints in such materials. Despite a wide range of empirical research, consideration of adhesive layers or surfaces in a structure is commonly done in a very simplified manner – they are often modelled as a perfect connection between adherends. It means the cohesive stiffness and opportunity of progressive delamination are neglected. This may lead to an overestimation of the structural load-bearing capacity. The article presents wood-wood and wood-carbon fibre reinforced polymer (CFRP) adhesively bonded joints' investigations, based on own experimental testing technique (covering a current one as a Digital Image Correlation), analytical double-lap model for adhesives and advanced numerical Finite Element approach. The aim of the paper is to give the guidelines for complex, non-linear modelling of connections in glue laminated timber and wood-CFRP composites that can be utilised for many purposes.

Keywords: FE analysis, adhesively bonded joints, wood-wood joints, Wood-CFRP joints, double-lap connection, cohesive stiffness and strength, delamination.

INTRODUCTION

Carbon Fibre Reinforced Polymer (CFRP) composites are still getting on popularity. The main reasons are their low weight and both high rigidity and strength. In timber constructions, they are primarily used to enhance existing load bearing members. Scientists do a variety of tests, where the example may be glued joints. Despite much research, such ties are often modelled as perfect. It means the cohesive stiffness and opportunity of progressive delamination are omitted. The literature is insufficient in guidelines for incorporating adhesive connections in wooden structures by exploiting such a current method as FE (Finite Element) analysis. There is only general information indicated. The author tries to decide which properties are necessary to be included in a numerical model. Simultaneous experimental investigations and computational analyses make it easier to be done. Subsequent steps are comprehensively reported. Some of them were established in the author's prior activities [1–4].

Tests on wood-wood and wood-CFRP adhesively bonded joints

Literature on general research on wood-wood and wood-CFRP adhesively bonded joints is extensive. Lavisci et al. proposed a method of testing joints in shear, applying tension or compression [5] according to the setup shown in Figure 1a. Gereke et al. [6] carried out numerical analyses of a similar lap joint in a glue laminated timber. Almeida et al. [7] and Cavalheiro et al. [8] tested a maximal shearing stress on the specimens composed of three elements, in a double-lap

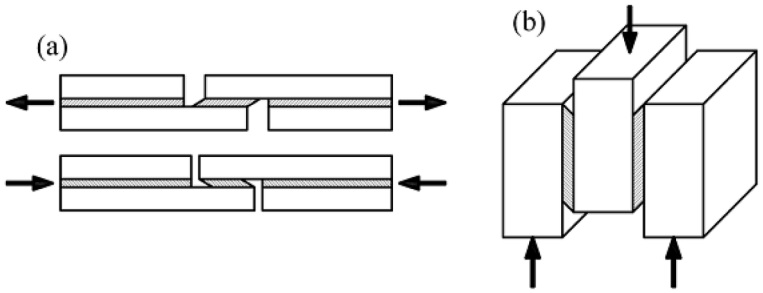

Figure 1. Configurations for testing lap joints in glue laminated timber [2]

configuration – as shown in Figure 1b. Rudawska et. al [9] analysed the influence on selected factors on the strength of wood adhesive joints.

Wang et al. [10] and Xu et al. [11] tried research on cracking of glue laminated timber on double cantilever beam (Figure 2a) and end notched flexure (Figure 2b) samples. Fortino et al. [12] performed numerical analyses of delamination in two samples – the first on the wedge-splitting (Figure 2c), and the second on a double cantilever beam (Figure 2a).

The next case is testing the joint in a wood-CFRP configuration. Many authors studied both single and double-lap joints of wood-CFRP. Vessby et al. [13], Wan et al. [14, 15], Biscaia et al. [16], Subhani et al. [17] and Vahedian et al. [18–21] examined strains redistribution in a single-lap joint between wood and CFRP plate (Figure 3a). Vessby et al. performed a numerical modelling, while Biscaia et al. and Vahedian et al. proposed an analytical solution. Biscaia et al. [22] extended the research with another double-lap scheme (Figure 3b).

Arriaga et al. [23] performed a block shear test (Figure 3c) with a GFRP (Glass Fibre Reinforced Polymer) Sena-Cruz et al. [24] and Fava et al. [25] carried out the pull-out test of two types of composite plates – GFRP and CFRP, glued on various lengths (Figure 3d). Lee et al. [26] presented the tests on CFRP strips separated from wood, as shown in Figure 3e.

In summary, scientists use a variety of static patterns to test wood-wood and wood-FRP connections. The lack of their systematisation and

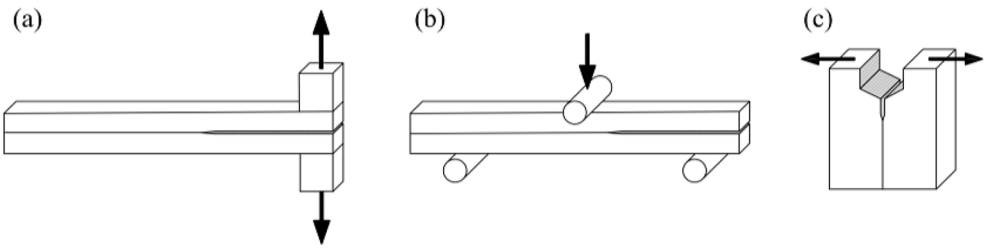

Figure 2. Methods for testing adhesively bonded wood-wood connections [2]

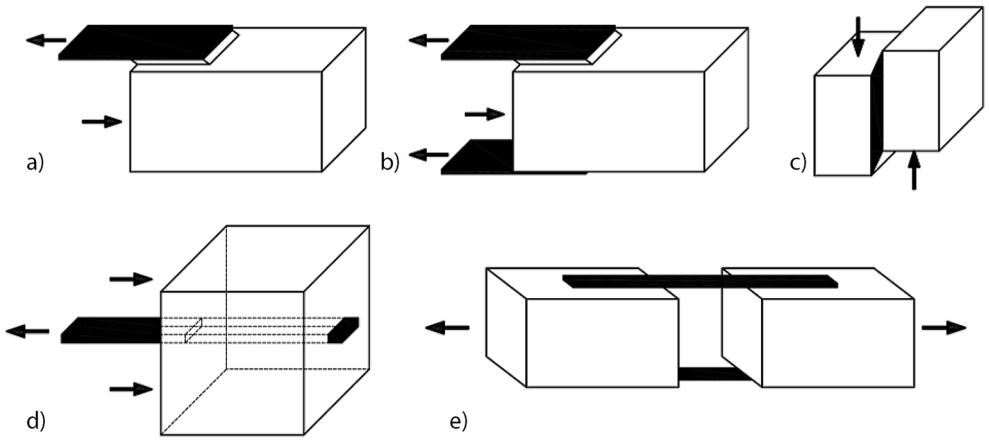

Figure 3. Methods for testing adhesively bonded wood-CFRP connections [2]

designation of the best method confirms the complexity of the problem.

Principles for FE modelling of adhesively bonded joints

Only single studies reporting FE modelling of glued wood and wood-containing composites have been detected in the literature. In two of them, connections between items were perfect [27, 28]. This means that phenomena taking place in a glued joint were neglected. Only Khelifa et al. [29] proposed modelling the adhesively bonded joint between CFRP and wood based on a cohesive surface, with the opportunity for delamination. According to the author of the paper, with non-linear analyses of glued elements comprising several layers, considering the stiffness of the adhesive and the opportunity of delamination between each of the layers is a key feature that substantially affects the results. The author recommended adopting practices for selecting the properties of the adhesive surface used in the mechanics of multi-layer composites, because of the lack of rules for the modelling joints in glue laminated timber structures.

The geometric thickness of the joint is small, so the cohesive elements or cohesive surfaces have, by definition, a unit constitutive thickness (t_{def}). As a result, the nominal strains are equal to the relative peeling displacements (1):

$$\varepsilon_n = \frac{\delta_n}{t_{def}}, \quad \varepsilon_s = \frac{\delta_s}{t_{def}}, \quad \varepsilon_t = \frac{\delta_t}{t_{def}} \tag{1}$$

If the uncoupled traction-separation law is used (2), each part of the adhesion stresses depends only on the nominal displacement and the corresponding cohesive stiffness of the joint (default method). It means the forces toward shearing are unaffected by peeling and inversely. The dependence is more complex when the coupled formulation is used (3).

$$\begin{Bmatrix} \sigma_n \\ \sigma_s \\ \sigma_t \end{Bmatrix} = \begin{bmatrix} K_{nn} & 0 & 0 \\ 0 & K_{ss} & 0 \\ 0 & 0 & K_{tt} \end{bmatrix} \begin{Bmatrix} \delta_n \\ \delta_s \\ \delta_t \end{Bmatrix} \tag{2}$$

$$\begin{Bmatrix} \sigma_n \\ \sigma_s \\ \sigma_t \end{Bmatrix} = \begin{bmatrix} K_{nn} & K_{ns} & K_{nt} \\ K_{ns} & K_{ss} & K_{st} \\ K_{nt} & K_{st} & K_{tt} \end{bmatrix} \begin{Bmatrix} \delta_n \\ \delta_s \\ \delta_t \end{Bmatrix} \tag{3}$$

The above rule applies to both the cohesive surface and the cohesive elements approach. The first method was used, among others, by Ramamurthi et al. [30], Needleman [31] and Ali et al. [32]. This approach, however, is based on the phenomenon of contact and works well in simple models. With a more complicated example, automatic stabilisation is necessary – by adding a variable whose impact should be carefully analysed. In addition, as the name suggests, automatic means much less control on it.

Thus, the second approach was chosen in the conducted investigations, much more often used by many authors, such as Camanho et al. [33], Song et al. [34], Moslemi and Khoshravan [35], Lepore and Perrella [36], de Moura et al. [37], Stuparu and Constantinescu [38], Mohammadi and Salimi-Majd [39], Soroush et al. [40] or Sitnikova et al. [41]. Cohesive elements offer the stability of the model from the very beginning of the analysis and only demand introducing artificial viscosity as delamination progresses. Its value and influence on calculations can be precisely controlled. Works on studies on this parameter exist in the literature, which makes a right choice easier. The eight-node COH3D8 cohesive element [33] was shown in Figure 4.

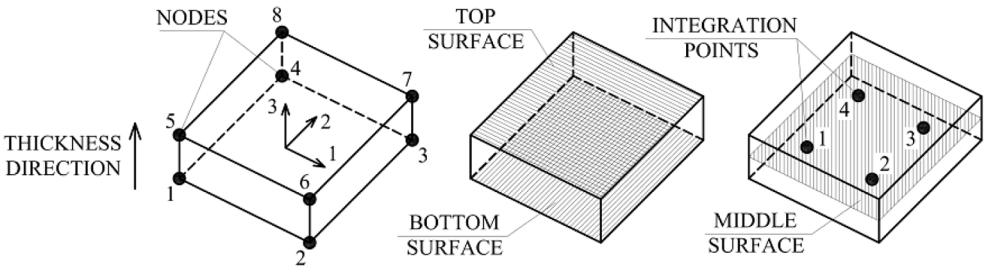

Figure 4. Cohesive element COH3D8

It is significant to set a correct thickness direction, which should correspond to axis no. 3. It can be done by specifying the bottom and top surfaces. Based on this, the central surface is established and the cuboidal element is transformed into a shell element. The dimension of a single cohesive element (l_e) should satisfy three conditions (4):

$$l_e \le \frac{l_{Ic}}{N_e}, \quad l_e \le \frac{l_{IIc}}{N_e}, \quad l_e \le \frac{l_{IIIc}}{N_e} \tag{4}$$

The length of the cohesive zone (l_{Ic}, l_{IIc}, l_{IIIc}) in the subsequent cracking modes should be calculated according to the formulas (5):

$$l_{Ic} \le ME_a \frac{G_{Ic}}{\sigma_{Ic}^2}, \quad l_{IIc} \le ME_a \frac{G_{IIc}}{\tau_{IIc}^2}, \quad l_{IIIc} \le ME_a \frac{G_{IIIc}}{\tau_{IIIc}^2} \tag{5}$$

Calculation of crack initiation stresses (σ_{Ic}, τ_{IIc}, τ_{IIIc}) is possible when dimensions of the finite element and transformations of the formulas (5) are done. It allows to reduce the number of elements with large structures. This approach was used by Turon et al. [42], based on conclusions drawn by Alfano and Crisfield [43]. Using the most commonly used Hillerborg theory (M = 1), the formulas are as follows (6):

$$\sigma_{Ic} = \sqrt{\frac{E_a G_{Ic}}{N_e l_{e,def}}}, \quad \tau_{IIc} = \sqrt{\frac{E_a G_{IIc}}{N_e l_{e,def}}}, \quad \tau_{IIIc} = \sqrt{\frac{E_a G_{IIIc}}{N_e l_{e,def}}} \tag{6}$$

Table 1. "*M*" parameter depending on a cohesive zone model.

Author of the model	*M*
Hui	0.21
Irwin	0.31
Dugdale, Barenblatt	0.40
Rice, Falk	0.88
Hillerborg	1.00

The most suitable number of elements in the cohesive zone (N_e) was not precisely defined. Many authors in their works use a different number between 2÷5 [44, 45]. Thus, choosing the number of elements depends on the analysed case.

Two criteria for damage initiation are available in the Simulia ABAQUS software [46] – maximal stress *Maxs* and quadratic *Quads* (7).

$$Maxs: \max\left(\frac{\sigma_{33}}{\sigma_{Ic}}, \frac{\tau_{13}}{\tau_{IIc}}, \frac{\tau_{23}}{\tau_{IIIc}}\right) = 1$$
$$Quads: \left(\frac{\sigma_{33}}{\sigma_{Ic}}\right)^2 + \left(\frac{\tau_{13}}{\tau_{IIc}}\right)^2 + \left(\frac{\tau_{23}}{\tau_{IIIc}}\right)^2 = 1 \tag{7}$$

However, the course of delamination can be carried out for two mixed energy criteria (8), considering energy release rates in respective modes (G_{Ic}, G_{IIc}, G_{IIIc}). The first was developed by Wu and Reuter [47], the second by Benzeggagh and Kenane [48].

$$Wu: G_c = \left(\frac{G_I}{G_{Ic}}\right)^\zeta + \left(\frac{G_{II}}{G_{IIc}}\right)^\zeta + \left(\frac{G_{III}}{G_{IIIc}}\right)^\zeta$$
$$BK: G_c = G_{Ic} + (G_{IIc} - G_{Ic})\left(\frac{G_{II} + G_{III}}{G_I + G_{II} + G_{III}}\right)^\eta \tag{8}$$

Next, the artificial viscosity should be introduced into the model. It allows for the convergence of the calculations in terms of material softening and its failure. Degradation progress is applied according to the following relationship (9):

$$d_\chi = \frac{1}{\chi}(d - d_\chi) \tag{9}$$

A viscosity parameter improves the stability of a model during progressive delamination, but an inappropriate value may significantly change the results and cause them to differ from reality. Its value in the paper was selected based on several recent publications, including Panettieri et al. [49], Abdulla et al. [50], Zoghbi [51] and Demir et al. [52]. In the cited works, the coefficient was assumed in a wide range χ = 0.00001÷0.002. Finally, one should consider how a degradation parameter d acts. It is known that it varies in the

range $d = 0 \div 1$, where 0 means no degradation, and 1 – full degradation. This parameter is calculated based on corresponding displacements, according to the relationship (10) presented by Camanho et al. [33]:

$$d(\delta) = \frac{\delta_f(\delta - \delta_0)}{\delta(\delta_f - \delta_0)} \tag{10}$$

Based on Figure 5, the value of δ_0 can be calculated using the known softening initiation stresses σ_0 and the cohesive stiffness of the adhesively bonded joint $K = K_a$. Denoting the energy released from the connection until the crack initiation as G_0, the value of the energy remaining from the softening initiation up to damage is $G_f = G_c - G_0$. It should be noted that G_c is the material property defined at the start of the analysis. Knowing the value of G_f, calculating the complete degradation displacement value δ_f is possible (11).

$$\begin{gathered} \delta_0 = \frac{\sigma_0}{K_a} \;\Rightarrow\; G_0 = \frac{1}{2}\sigma_0\delta_0 \;\Rightarrow \\ \Rightarrow\; \delta_f = \frac{2(G_c - G_0)}{\sigma_0} + \delta_0 \end{gathered} \tag{11}$$

The graph shown in Figure 5 can be prepared, after the degradation parameter is made dependent on the current displacement δ (11).

MATERIALS AND METHODS

Several methods of testing adhesively bonded joints were outlined in Section 1.1 of the article. However, in the author's opinion, only one of them was appropriate for the investigations. Polyurethane adhesive fulfills its role as a strong connection only when the thickness of the bonding layer is insignificant. This can be provided by gluing adherends under high pressure, as during glue laminated timber load-bearing elements production. Compliance with the technological regime is essential for gaining actual properties of the adhesive. Because of that, testing specimens cut directly from structural beams should let to transfer results from the analysed double-lap shear connection to full-scale load-bearing members.

Description of the specimens and experimental setup

18 glue laminated timber small blocks with dimensions of 120×74×93 mm and 18 wood-CFRP composite small blocks with dimensions of 123×74×93 mm were formed by cutting beams produced from GL24h glue laminated timber class by ABIES Poland Ltd. with the usage of CFRP tapes C-Laminate SM 100/1.4 made by S&P Poland Ltd. A gluing process of the beams in ABIES Poland Ltd. is presented in Figure 6 and exemplary wood-wood (K) and wood-CFRP (KW) specimens in Figure 7 and Figure 8, consecutively.

The experiments were executed on the MTS 809 testing machine, which registered the applied force (P). Displacement measurements were conducted employing the DIC (Digital Image Correlation) method, which enabled to follow the samples' work up to their failure (Figure 9). A black and white stochastic pattern (otherwise called – random points) allowed to read the value of displacements in every point of the specimen and, as an effect, to measure it in the middle of the adherends. The camera used in measurements was Panasonic HC-X1000, which recorded images in resolution 3840×2160 pixels with frequency 60 frames per second. GOM Correlate program was used to develop the displacements and strains results in 2D space.

Next, preparing pictures with deformations distribution was possible. They were utilised for correlating results between experiments and FE computations.

FE models details

Fully non-linear FE model involves rigid criteria for the mesh size and types of finite elements, which should be undertaken when the model formulation begins. This try makes it comfortable to manage highly mesh dependent phenomena as plasticity or delamination. It supports transferring the gathered results between consecutive models if the established mesh rules are followed. The mesh size should be relatively easily applicable to larger structures than the one analysed – the principles described in Section 1.2 should be pursued. In the paper, to prepare the model and compute the results, Simulia ABAQUS 2019 software was used [46]. Calculations of the model were performed with Abaqus/Standard implicit solver.

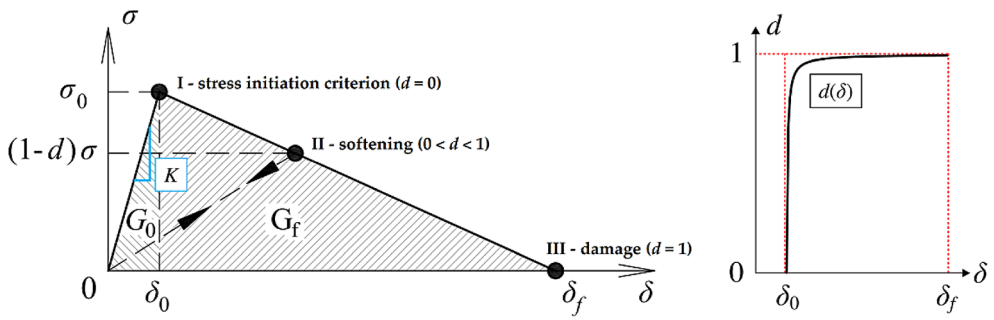

Figure 5. Constitutive law of material with linear softening and degradation parameter

Figure 6. Process of gluing load-bearing beams in ABIES Poland Ltd. and prepared specimens

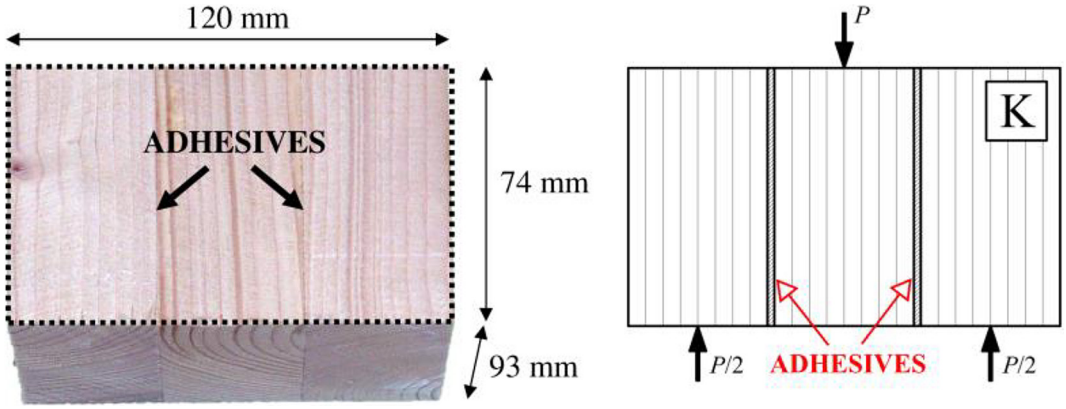

Figure 7. Exemplary wood-wood specimen (K)

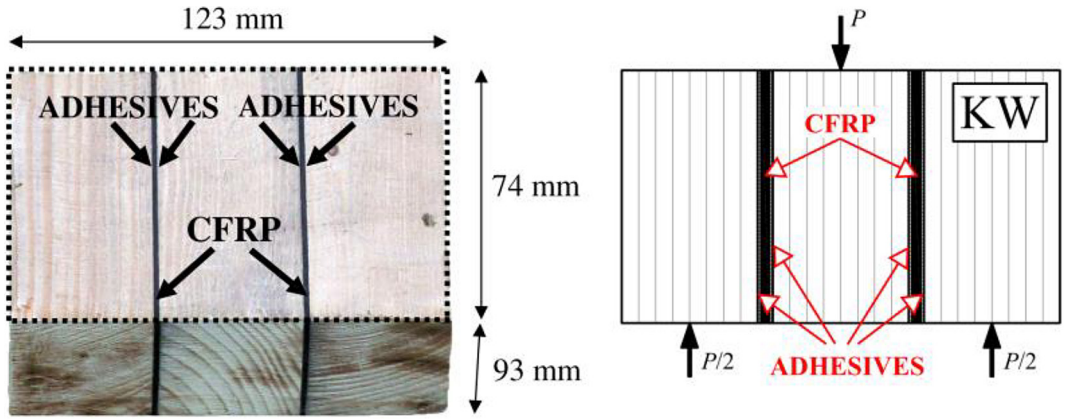

Figure 8. Exemplary wood-CFRP specimen (KW)

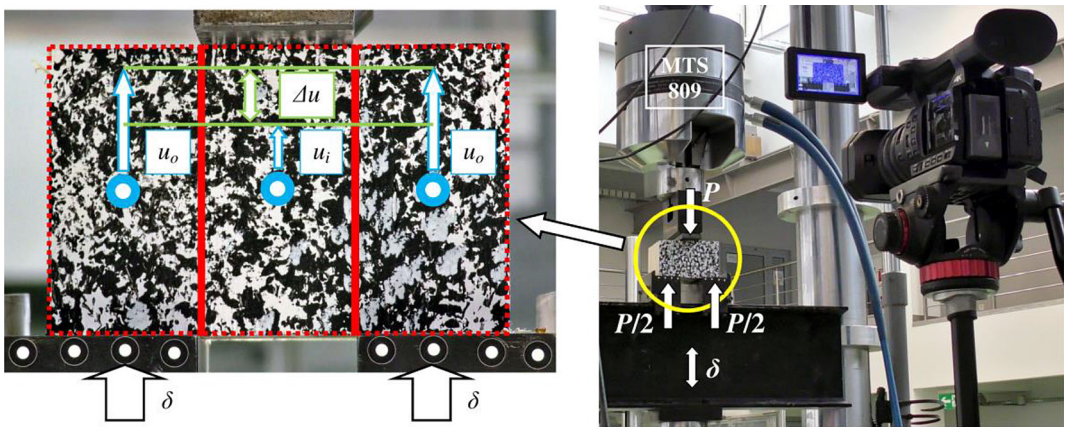

Figure 9. Experimental setup and denotations of displacements

Conforming to the assumptions done in earlier author's work [1–4], wood should be modelled with C3D20 elements in a cubic shape with a side of 10 mm. The size of the cohesive elements should be selected, preserving the principle of at least one finite element between the nodes of the adherends' elements [46]. Assuming wood modelling using C3D20 elements, the dimension of the COH3D8 cohesive element will be 5 mm × 5 mm. CFRP tape should be modelled with shell CSS8 elements, with dimensions of 5 mm × 5 mm, formulated by Vu-Quoc [53].

In order to predict the failure of the part materials, anisotropic Hill's perfect plasticity was applied both to wood and CFRP tapes and linear softening law to adhesively bonded joints. Summarised properties of wood and CFRP are collected in Table 2, while for glued joint were gathered in Tables 4 and 5 in the consecutive Sections. Symmetry of the sample by its centre was assumed, which allowed modelling only the half (Figure 10) and provided simplified and faster computations.

Determination of cohesive stiffness necessary to be applied to the FE model

Determination of cohesive stiffness, demanded to be implemented as a property of cohesive elements, was based on a double-lap analytical model formulated by Tsai [54–56]. The dimensions, materials' properties (Figure 11 and Table 3) and relative displacement *Δu* (Figure 9) are known. Then calculating cohesive stiffness [2, 3], both for glue laminated timber and wood-CFRP samples, using formulas (12–13), is possible.

$$K_{a,K}(\Delta u)=\frac{1}{\frac{2\Delta u}{P}bL_a-\frac{h_L}{2G_{12}}-\frac{L_a^2}{h_L E_1}}$$
$$K_{a,KW}(\Delta u)=\frac{1}{\frac{\Delta u}{P}bL_a-\frac{h_L}{4G_{12}}-\frac{L_a^2}{2h_L E_1}-\frac{t_W}{2G_W}} \quad (12)$$

Determination of properties for progressive delamination in wood-wood joint

First, only the wood-wood joint was examined. It enabled to exploit directly the Tsai model to justify FE model assumptions. Afterward, properties for wood-CFRP connection were analysed numerically and contrasted with the experimental results. The cohesive stiffness of the adhesive

Table 2. Properties of wood and CFRP applied to the numerical model

Parameter	Wood	CFRP
E_1 (GPa)	11.439	175
E_2 (GPa)	0.732	7.1
E_3 (GPa)	0.458	
G_{12} (GPa)	0.715	2.73
G_{13} (GPa)	0.529	
G_{23} (GPa)	0.690	
v_{12} (/)	0.335	0.3
v_{13} (/)	0.358	
v_{23} (/)	0.416	
f (MPa)	61.17	2800
R_{11} (/)	0.569	1
$R_{22} = R_{33}$ (/)	0.040	0.025
$R_{12} = R_{13} = R_{23}$ (/)	0.206	0.016

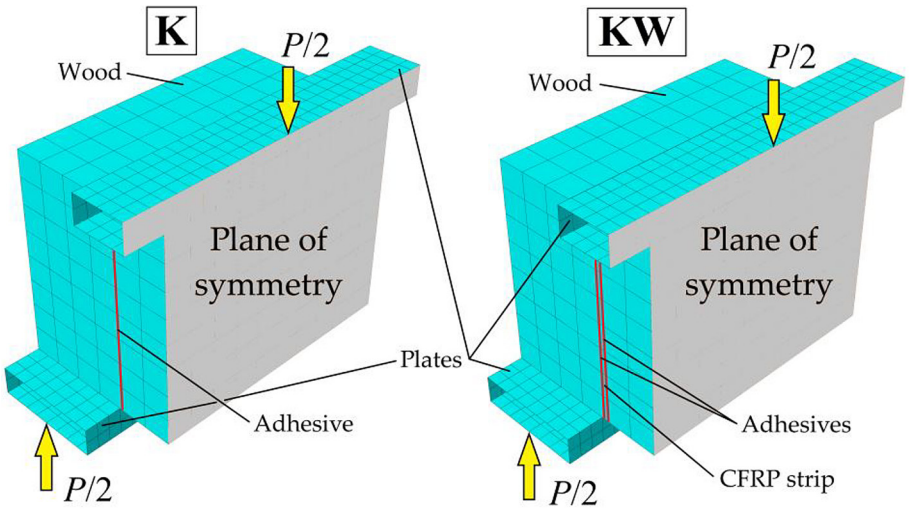

Figure 10. FE model – mesh and description of the parts

surface with the value $K_{a,K}$ = 91.32 MPa/mm, resulting from the formula (12), was introduced into the model. Checking the results from the numerical model was unavoidable because of the vast number of variables. In the linear-elastic range, the shear stresses in a joint were supposed to correspond to the same stresses calculated from the analytical model. The Tsai double-lap shear model, after introducing simplifications resulting from the examined case, provided shear stress values based on the formulas (13–14) – according to denotations shown in Figure 12.

$$\tau_a(x) = A\sinh(\beta x) + B\cosh(\beta x),$$
$$\tau_{avg} = \frac{P}{A_v} = \frac{P}{4bc} \tag{13}$$

$$A = \frac{\beta c \tau_{avg}}{3\cosh(\beta c)}, \quad B = \frac{\beta c \tau_{avg}}{\sinh(\beta c)},$$
$$\beta = \sqrt{\frac{3K_a}{E_1 h_L\left(1 + \frac{K_a h_L}{2G_{12}}\right)}} \tag{14}$$

To analyse the results, an adhesive surface with shear stresses corresponding to Tsai proposal was isolated from the FE model (Figure 13).

The second step involved resolving stresses on the edge and in the middle of the joint divided by the average shear stresses (τ_{avg}). Afterward, the results from FE computations were juxtaposed with the results from the Tsai model. Better agreement between these two was seen at the centre than at the joint's edge, which derived from a plane stress presumption in analytical examinations. The presented investigation confirmed the correct assumptions of the FE model reflecting the analytical solution.

The adherends analysed in the paper were fastened using polyurethane (PUR) glue, because of its widespread usage in producing glue laminated timber. Detailed studies of material properties of several types of PUR adhesives were presented, among others, by Klausler et al. [57] and Clauß et al. [58]. Their research shows that these adhesives have a shear modulus as wood, which allows avoiding a shear stresses concentration in a joint. In addition, during the gluing of the lamellas, an adequately high pressure is ensured, which enables to get a joint of a negligible thickness – typically around t_a = 0.1 mm. An average modulus of elasticity of PUR adhesives can be estimated as E_a = 1.2 GPa. The critical values of the energy release rates for wood fastened with polyurethane glue in the modes were taken from Xu et al. [11] and are G_{Ic} = 85 J/m² and $G_{IIc} = G_{IIIc}$ = 820 J/m², respectively. A viscosity coefficient was assumed at the level of χ = 0.0005, based on the work of Demir et al. [52], who investigated the accuracy of the results got at distinct viscosity coefficients and its impact on the convergence of computations. Accepting the approach of Hillerborg et al. [59], Falk et al. [44] and the work of Turon et al. [42] for a finite element with dimensions of 5 × 5 mm and 2 elements in the cohesion zone, the values of crack initiation stresses are (15):

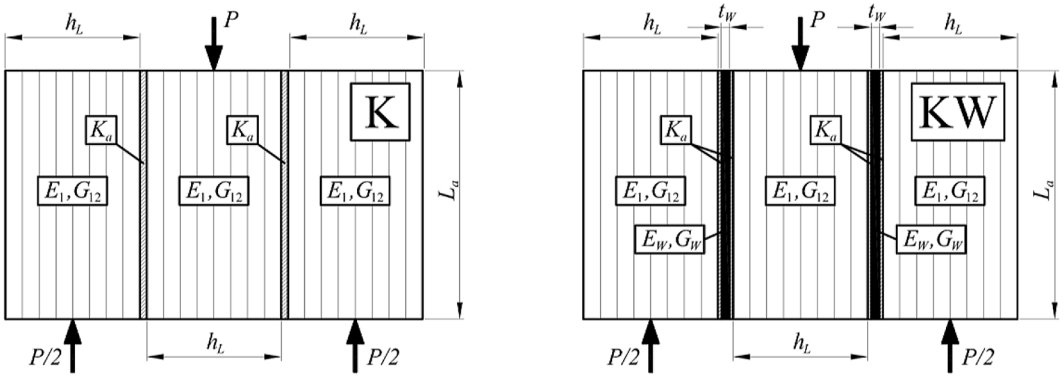

Figure 11. Denotations used in Tsai double-lap connection model

$$\sigma_{Ic} = \sqrt{\frac{E_a G_{Ic}}{N_e l_{e,def}}} = 3.19\,\mathrm{MPa},$$
$$\tau_{IIc} = \tau_{IIIc} = \sqrt{\frac{E_a G_{IIc}}{N_e l_{e,def}}} = 9.92\,\mathrm{MPa} \quad (15)$$

In the current paper, the quadratic stress initiation criterion (*Quads*), represented in Section 1.2 by formula (7), was utilised. It is considerably more often used by scientists. Similarly, the mixed energy (*BK*) criterion was selected – formula (8). Properties necessary to do complete calculations are collected in Table 4.

Applying the above properties, computations were executed to resolve complete delamination, regarded as a full loss of joint stiffness. The curve from FE calculations related to the average curve and its standard deviations from experimental investigations for "K" specimen are shown in Figure 14.

The linear-elastic stiffness of the setup got in the FE model was $K_{a,K,FEA}$ = 270.36 kN/mm, while in experiments $K_{a,K,EXP}$ = 269.87 kN/mm, which means compliance up to 0.2%. Similarly, the maximal force prediction was highly exact, because a relative variation did not exceed 2.5%.

Determination of properties for progressive delamination in wood-CFRP joint

When analysing the wood-CFRP joint, it was unavoidable to regulate the critical values of energy release rates and crack initiation stresses. After computing cases for particular cohesive stiffness, according to formula (11) – $K_{a,K}$ = 91.32 MPa/mm and $K_{a,KW}$ = 49.51 MPa/mm, the same calculation step was chosen in each case and the shearing stresses in adhesive surfaces were compared. The maximal stresses at the applied wood-CFRP stiffness accounted for 70% of the stresses at the wood-wood stiffness. Accepting an analogous relationship to crack initiation stresses, it was possible to adjust the relevant critical values of the energy release rates (16–17):

$$\sigma_{Ic}^{\ red} = 0.7\sigma_{Ic} = 2.23\,\mathrm{MPa},$$
$$\tau_{IIc}^{\ red} = 0.7\tau_{IIc} = 6.94\,\mathrm{MPa} \quad (16)$$

$$G_{Ic} = \frac{(0.7\sigma_{Ic})^2 N_e l_{e,def}}{E_a} = 42\,\frac{\mathrm{J}}{\mathrm{m}^2},$$
$$G_{IIc} = \frac{(0.7\tau_{IIc})^2 N_e l_{e,def}}{E_a} = 402\,\frac{\mathrm{J}}{\mathrm{m}^2} \quad (17)$$

The parameters used for the final numerical model are listed in Table 5. Comparison of the results from the FE model with experiments is shown in Figure 15.

The introductory linear-elastic stiffness of the setup in the FE model was

Table 3. Properties and dimensions used in the Tsai model.

Parameter	Value
E_1	11.439 GPa
G_{12}	0.715 GPa
G_W	2.730 GPa
b	93 mm
h_L	40 mm
t_W	1.4 mm
L_a	74 mm

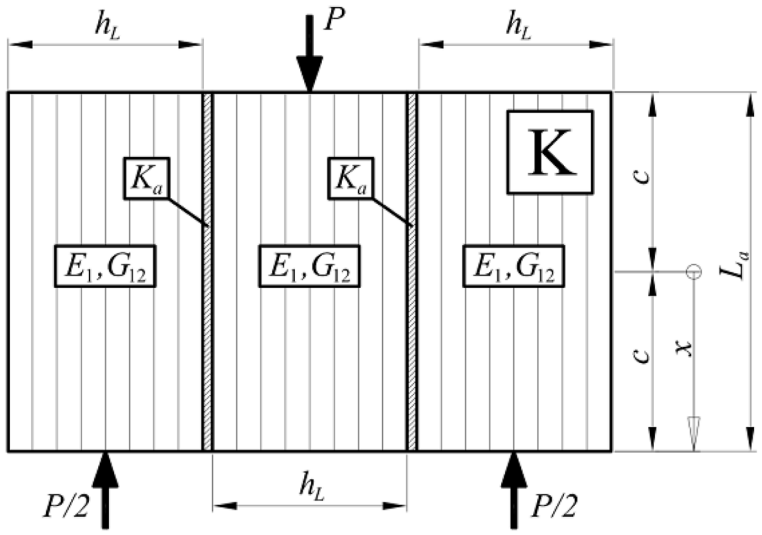

Figure 12. Denotations according to Tsai model shearing stresses calculation

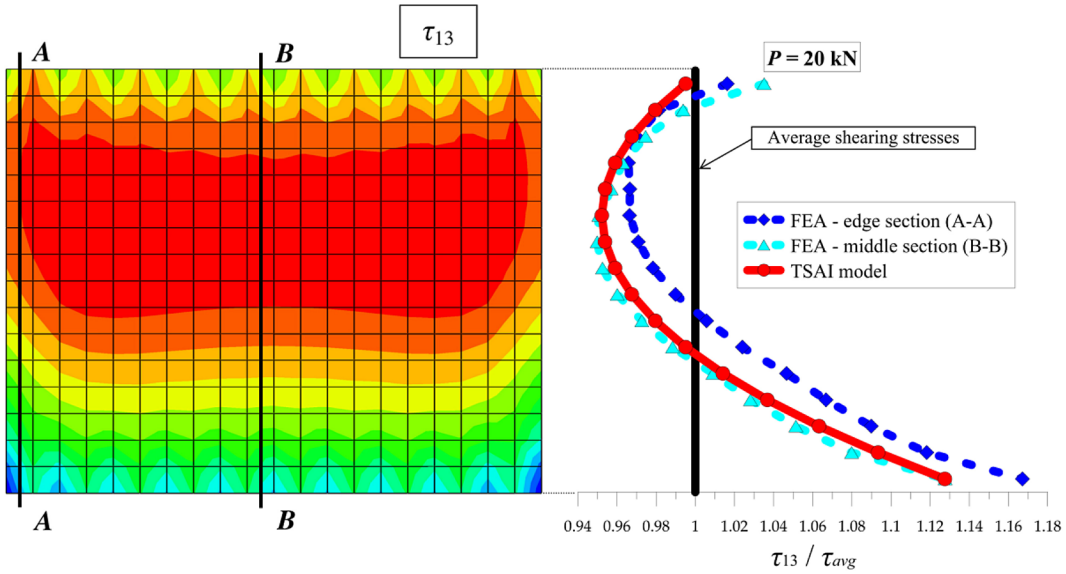

Figure 13. The adhesive surface isolated from the FE model and comparison to Tsai shearing stresses

$K_{a,KW,FEA}$ = 173.18 kN/mm, while experimental $K_{a,KW,EXP}$ = 170.29 kN/mm. It means fewer than 2% of relative variation. At a subsequent stage (from a force of 20 kN), the slope of an average empirical curve steadily increased. The discrepancy could arise from the asymmetry or inaccuracy in cutting the specimens. The maximal force agreement was achieved with an accuracy of 1.9%.

Table 4. Parameters for wood-wood connection FE modelling

Parameter	Value
$K_a = K_{nn} = K_{ss} = K_{tt}$	91.32 MPa/mm
σ_{Ic}	3.19 MPa
$\tau_{IIc} = \tau_{IIIc}$	9.92 MPa
G_{Ic}	85 J/m^2
$G_{IIc} = G_{IIc}$	820 J/m^2
η	1.8
χ	0.0005

Table 5. Parameters for wood-CFRP connection FE modelling

Parameter	Value
$K_a = K_{nn} = K_{ss} = K_{tt}$	49.51 MPa/mm
σ_{Ic}	2.23 MPa
$\tau_{IIc} = \tau_{IIIc}$	6.94 MPa
G_{Ic}	42 J/m^2
$G_{IIc} = G_{IIc}$	402 J/m^2
η	1.8
χ	0.0005

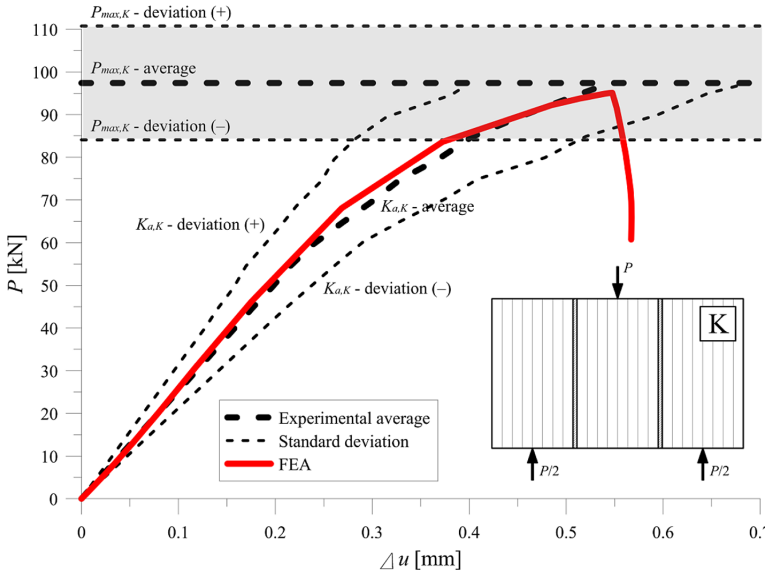

Figure 14. Experimental and numerical results for K samples

RESULTS AND DISCUSSION

The FE model, under the assumptions used, predicted a rapid destruction of the specimen because of adhesively bonded joint cracking. Wood degradation processes were described by its progressive plasticisation. In each of the analysed samples, the form of damage was mixed. Shearing occurred in the adhesive or in the wood in its vicinity. The DIC technique enabled to find the places of significant distortion of the stochastic pattern. Thus, it was possible to show the zones where the plasticisation began. Dividing results into failure due to tension, compression or shear was problematic because the plasticity was expressed with Hill's theory, which makes it impossible to distinguish them. In order to correlate the results from the DIC method with the FE computations, deformations at which plasticisation may occur were evaluated. Then the average value was estimated (18), as considered exact enough.

$$\varepsilon_{DIC} = \frac{1}{3}\left(\frac{f_{c,1}}{E_1} + \frac{f_{c,2}}{E_2} + \frac{f_{v,12}}{G_{12}}\right) = 0.611\% \quad (18)$$

Because of the high anisotropy of wood, matching individual empirical deformations with the FE model was not justified. The material is usually homogenised to follow the average values. Strict identification of the DIC results in the FE computations could be achievable only if individual properties of each lamella were introduced and each fibre, knot, and other wood defects distorting the deformation distribution were modelled. In addition, the experimental results were characterised by a significant dispersion of the destructive force and relative displacements and only one specimen surface was observed, which made such a thorough analysis impossible.

First, the wood-wood connection was presented. The most representative examples were selected and presented in Figure 16. Plasticised regions, according to the formula (17), were marked with red and blue colour based on the averaged values of stochastic pattern deformations.

In order to relate the FE computations to the DIC results, one specimen was chosen and thoroughly analysed (Figure 17). The red and blue colours from the DIC results illustrate deformation of the pattern, representing the plasticisation of the wood. The red colour from the FE model means full plasticisation, calculated based on the Hill's theory, while in the adhesive it means full loss of stiffness. Four regions can be distinguished:

- A – tension zone in the middle part – similar location in both cases. However, it has a smaller range in the FE model than in the experiment,
- B – shear zone along the joint, where yielding is similar,
- C – crushing zones at the points of support. The FE model, however, better reflects the plasticisation in the top support vicinity,
- D – zone of full delamination of the connection. The joint failure is the same.

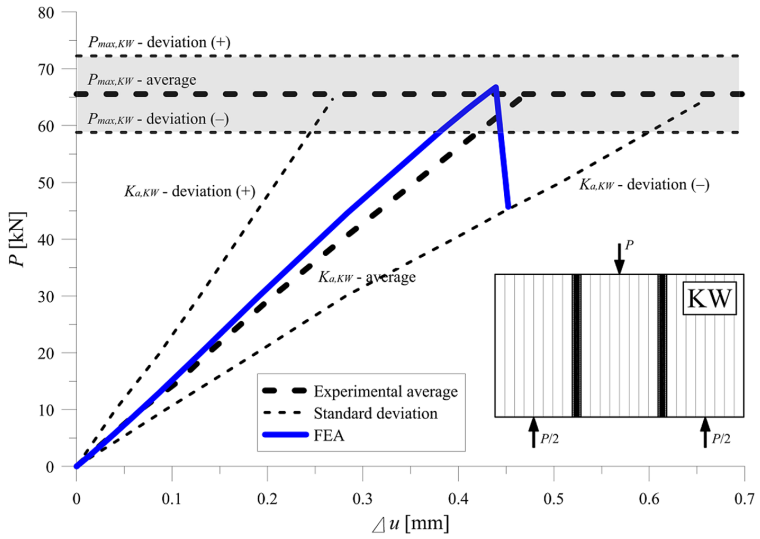

Figure 15. Experimental and numerical results for KW samples

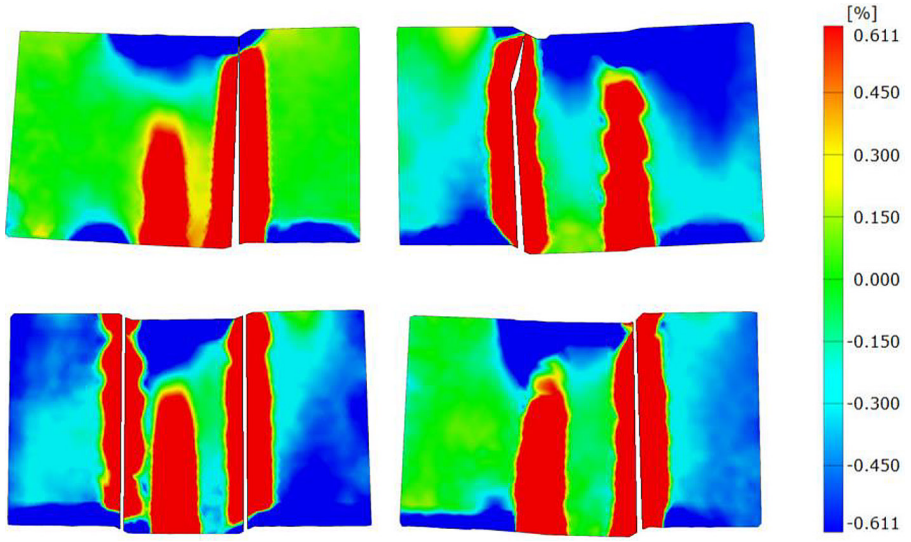

Figure 16. Representative examples from DIC method for K specimens (wood-wood)

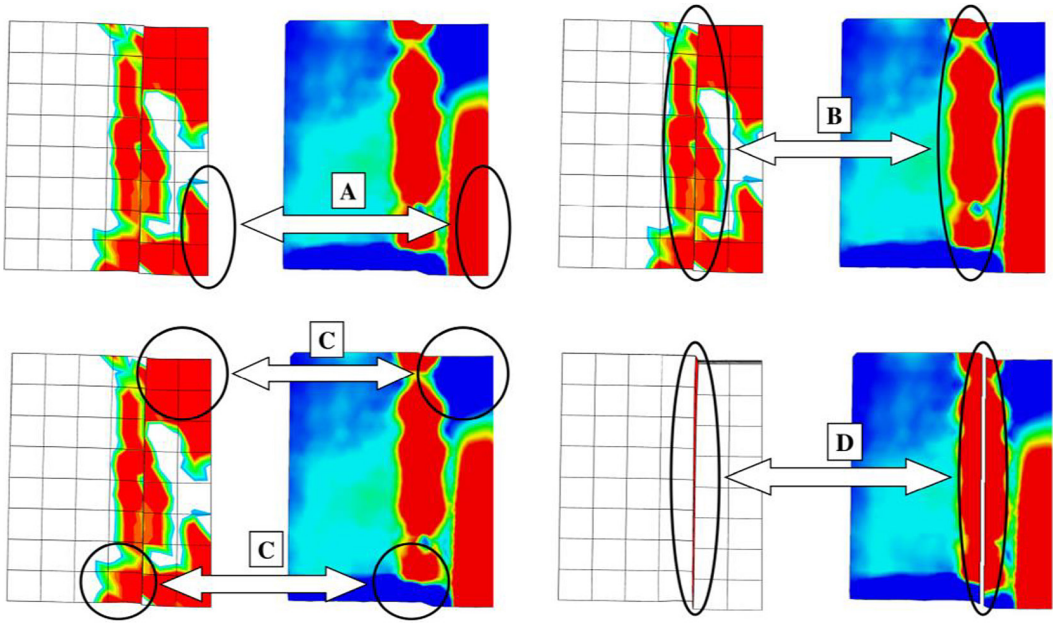

Figure 17. Comparison between DIC and FE results for K samples (wood-wood)

Worth mentioning is that, to show a crack in the FE model, defining connection stiffness degradation is necessary. The elements are gradually disconnected until they become independent of each other. The DIC method invariably treats the pattern as one connected element, so the strains increase constantly. Thus, the last phase should be interpreted only in terms of failure form.

Second, the wood-CFRP connection was analysed. As before, the most representative examples were selected and presented in Figure 18. Similar principles for graphical presentation were applied.

The FE model is compared to the DIC results in Figure 19. Three regions can be distinguished:

- A – tension zone in the middle part – similar location in both cases,
- B – crushing zones at the points of support. The FE model, however, better reflects the plasticisation in the top support vicinity,
- C – zone of full delamination of the connection. The joint failure is the same.

CONCLUSIONS

Despite a wide range of empirical research, consideration of adhesive layers or surfaces in a structure is commonly done in a very simplified manner – they are often modelled as a perfect

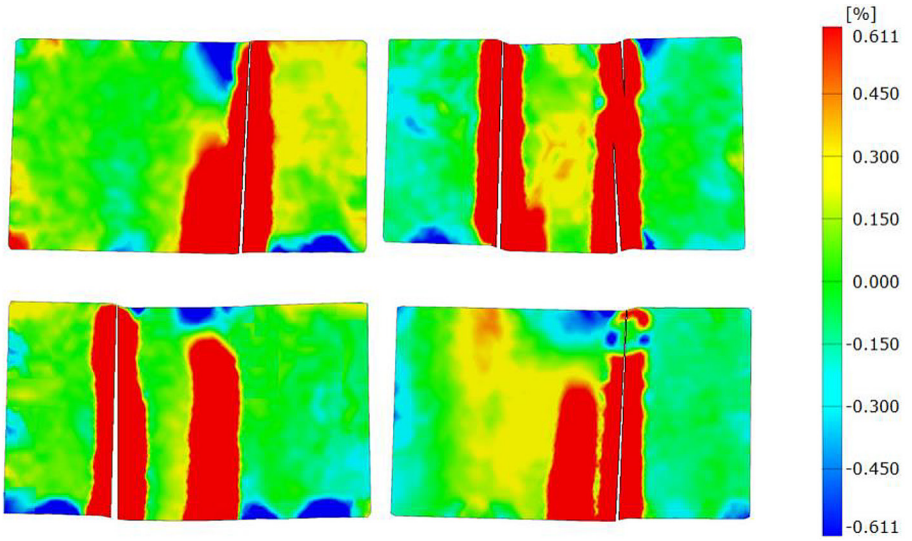

Figure 18. Representative examples from DIC method for KW specimens (wood-CFRP).

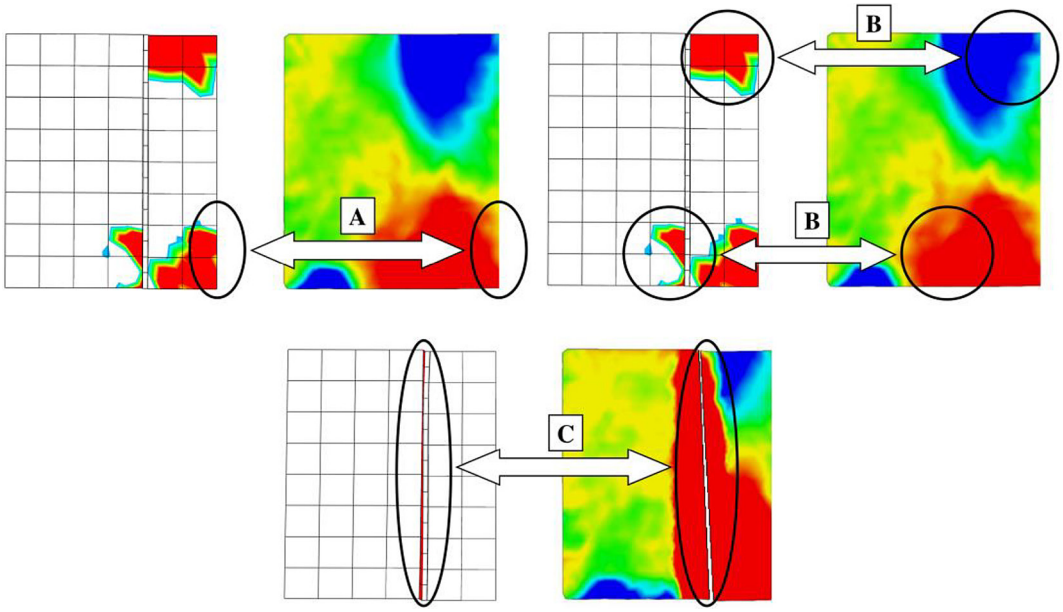

Figure 19. Comparison between DIC and FE results for KW samples (wood-CFRP)

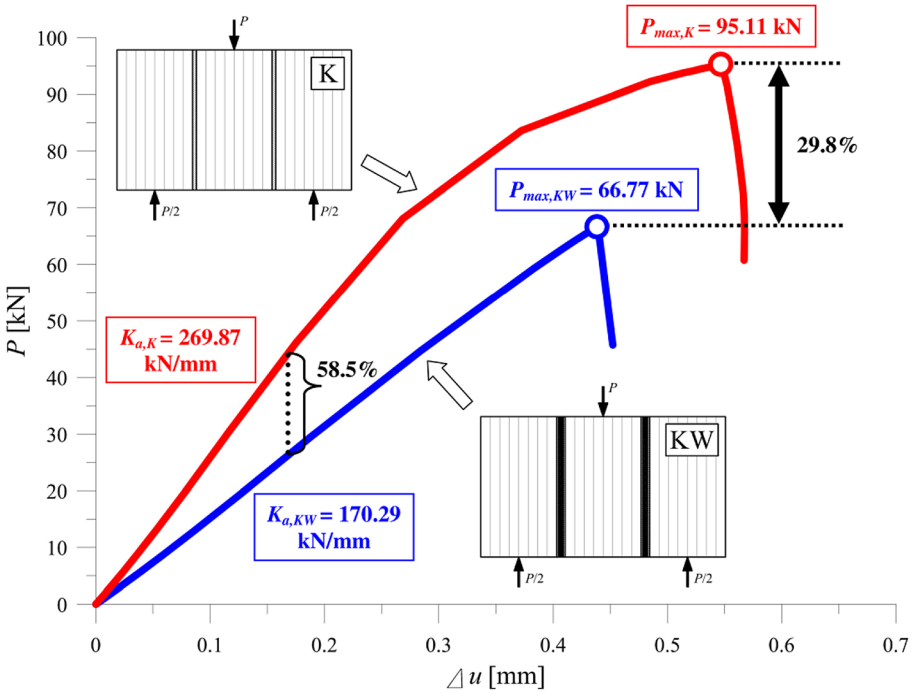

Figure 20. Stages of Experimental (DIC) and numerical results for KW samples

connection between adherends. It means the cohesive stiffness and opportunity of progressive delamination are neglected. This may lead to an overestimation of the structural load-bearing capacity.

To confirm this statement, a cumulative chart was provided (Figure 20). It illustrates the force-displacement curves for both cases (wood-wood and wood-CFRP). Studying the results of the maximal force got for both types of investigated samples, it can be concluded that the wood-CFRP adhesive is weaker by 30% than the wood-wood connection. Comparable situation is noticeable with joint stiffness, where wood-CFRP is 60% weaker.

Based on the current scientific literature, the methods of including adhesive stiffness and opportunity of progressive delamination were presented. FE computations agreed with the results got from a statistically valid number of samples in terms of force-displacement curves and forms of failure. The proposed models, despite many simplifications to reality, allow for sufficiently exact prediction of stiffness, maximal force and the form of failure of the tested elements.

The article presented wood-wood and wood-CFRP adhesively bonded joints' investigations, based on own experimental testing technique, analytical double-lap model for adhesives and advanced numerical Finite Element approach. The fact is that research was done only for polyurethane glue and behaviour of other glues may differ. Despite this, at least several general conclusions for experimental testing and non-linear modelling of connections in glue laminated timber and wood-CFRP composites may be stated. The elaborated experimental testing method concerns measurements in two-dimensional space that can be done on GOM Correlate software if a professional digital camera is available. Only high resolution ensures a correct determination of displacements or strains distribution. Standard frequency of recording as 50–60 frames per second is enough for gathering maximal force and displacement values. It is not appropriate for crack path tracing. Following thoroughly the rules on meshing the FE model provided by other scientists is extremely significant. Strong dependency on mesh size influences employing only accurately studied theories. This elaboration affirms that the size of a finite element for wood should be 10 mm and adhesive or CFRP tape – 5 mm. This produces an efficient transmission of the results to larger or more sophisticated models. Any variations from these proportions should be scrupulously investigated before the usage. One should note that these presumptions refer to Simulia ABAQUS program 2019 version or higher. Applying the suggested approach, an influence of the connection stiffness and opportunity of

delamination can be examined. One can calculate the designed model up to the moment of failure. Identifying the dangerous places where delamination may appear and how it affects the entire structure may be essential knowledge with non-obvious structures. Following the guidelines presented in the paper, one can analyse both wood-wood and wood-CFRP adhesively bonded joints with not very time-consuming computational effort. The ideas can be applied both to small and full-scale experimental-numerical analyses.

Acknowledgments

The research was done in Lublin University of Technology and supported under FD-20/IL-4/028 grant.

REFERENCES

1. Kawecki B., Podgórski J. 3D ABAQUS simulation of bent softwood elements. Archives of Civil Engineering 2020; 66: 323–337.
2. Kawecki B., Podgórski J. The effect of glue cohesive stiffness on the elastic performance of bent wood–CFRP Beams. Materials 2020; 13: 1–23.
3. Kawecki B. Selection of the parameters for numerical models of full girders made of wood-polymer composites reinforced with fibres (in Polish), Wydawnictwo Politechniki Lubelskiej, Lublin, Poland. http://bc.pollub.pl/dlibra/publication/13966, 2021.
4. Kawecki B. Guidelines for FEM modelling of wood-CFRP beams using ABAQUS, Archives of Civil Engineering 2021; 67: 175–191.
5. Lavisci P., Berti S., Pizzo B., Triboulot P., Zanuttini R. A shear test for structural adhesives used in the consolidation of old timber. Holz Als Roh- Und Werkstoff 2001; 59: 145–152.
6. Gereke T., Hering S., Niemz P. Finite element analysis of wood adhesive joints, Annals of Warsaw University of Life Sciences – SGGW. Forestry and Wood Technology 2015; 89: 36–49.
7. Henrique de Almeida D., Schmitt Cavalheiro R., Borges de Macêdo L., Calil Neto C., Luis Christoforo A., Calil Junior C., Antonio Rocco Lahr F. Evaluation of quality in the adhesion of glued laminated timber (Glulam) of paricá and lyptus wood species. International Journal of Materials Engineering 2014; 4: 114–118.
8. Cavalheiro R.S., Neto C.C., Christoforo A.L., Junior C.C., Lahr F.A.R. Evaluation of shear strength and cyclic delamination of paricá (schizolobium amazonicum) glued laminated timber. International Journal of Materials Engineering 2016; 6: 60–65.
9. Rudawska A., Maziarz M., Šajgalík M., Valášek P., Zlamal T., Iasnii V. The influence of selected factors on the strenght of wood adhesive joints. Advances in Science and Technology Research Journal 2018; 12: 47–54.
10. Wang V.Z., Ginger J.D., Narayan K. Intralaminar and interlaminar fracture characterization in glued-laminated timber members using image analysis. Engineering Fracture Mechanics 2012; 82: 73–84.
11. Xu B.H., Zhao Y.H., Guo J.H., Wang Y.X. Fracture toughnesses of interlaminar fracture of glued-laminated timber. Wood Research 2016; 61: 951–958.
12. Fortino S., Zagari G., Mendicino A. L., Dill-Langer G., A simple approach for FEM simulation of Mode I cohesive crack growth in glued laminated timber under short-term loading. Rakenteiden Mekaniikka (Journal of Structural Mechanics) 2012; 45: 1–20.
13. Vessby J., Serrano E., Enquist B. Contact-free measurement and numerical and analytical evaluation of the strain distribution in a wood-FRP lap-joint. Materials and Structures 2010; 43: 1085–1095.
14. Wan J., Smith S.T., Qiao P.Z. FRP-to-softwood joints: experimental investigation. In: 5th Int. Conf. FRP Compos. Civ. Eng., 2010; 1–5.
15. Wan J., Smith S.T., Qiao P., Chen F. Experimental investigation on FRP-to-timber bonded interfaces. Journal of Composites for Construction 2014; 18: 1–9.
16. Biscaia H.C., Cruz D., Chastre C. Analysis of the debonding process of CFRP-to-timber interfaces. Construction and Building Materials 2016; 113: 96–112.
17. Subhani M., Globa A., Al-Ameri R., Moloney J. Effect of grain orientation on the CFRP-to-LVL bond. Composites Part B: Engineering 2017; 129: 187–197.
18. Vahedian A., Shrestha R., Crews K. Bond strength model for externally bonded FRP-to-timber interface. Composite Structures 2018; 200: 328–339.
19. Vahedian A., Shrestha R., Crews K. Analysis of externally bonded Carbon Fibre Reinforced Polymers sheet to timber interface. Composite Structures 2018; 191: 239–250.
20. Vahedian A., Shrstha R., Crews K. Experimental investigation on the effect of bond thickness on the interface behaviour of fibre reinforced polymer sheet bonded to timber. International Journal of Structural and Construction Engineering 2018; 12: 1157–1163.
21. Vahedian A., Shrestha R., Crews K. Effective bond length and bond behaviour of FRP externally bonded to timber. Construction and Building Materials 2017; 151: 742–754.
22. Biscaia H.C., Chastre C., Cruz D., Viegas A. Prediction of the interfacial performance of CFRP

laminates and old timber bonded joints with different strengthening techniques. Composites Part B: Engineering 2017; 108: 1–17.

23. Arriaga F., Íñiguez-Gonzales G., Esteban M. Bonding shear strength in timber and GFRP glued with epoxy adhesives. Wood Research, 2011; 56: 297–310.
24. Sena-Cruz J., Jorge M., Branco J.M., Cunha V.M.C.F. Bond between glulam and NSM CFRP laminates. Construction and Building Materials 2013; 40: 260–269.
25. Fava G., Carvelli V., Poggi C. Pull-out strength of glued-in FRP plates bonded in glulam. Construction and Building Materials 2013; 43: 362–371.
26. Lee Y., Park J., Hong S., Kim S. A study of bond of structural timber and carbon fiber reinforced polymer plate. Materials Science 2015; 21: 563–567.
27. Nowak T.P., Jasieńko J., Czepiżak D. Experimental tests and numerical analysis of historic bent timber elements reinforced with CFRP strips. Construction and Building Materials 2013; 40: 197–206.
28. Glišović I., Pavlović M., Stevanović B., Todorović M. Numerical analysis of glulam beams reinforced with CFRP plates. Journal of Civil Engineering and Management 2017; 23: 868–879.
29. Khelifa M., Auchet S., Méausoone P.-J., Celzard A. Finite element analysis of flexural strengthening of timber beams with Carbon Fibre-Reinforced Polymers. Engineering Structures 2015; 101: 364–375.
30. Ramamurthi M., Lee J.-S., Yang S.-H., Kim Y.-S., Delamination characterization of bonded interface in polymer coated steel using surface based cohesive model. International Journal of Precision Engineering and Manufacturing 2013; 14: 1755–1765.
31. Needleman A. Some issues in cohesive surface modeling, Procedia IUTAM 2014; 10: 221–246.
32. Ali A., Lo Conte A., Biffi C.A., Tuissi A. Cohesive surface model for delamination and dynamic behavior of hybrid composite with SMA-GFRP interface, International Journal of Lightweight Materials and Manufacture 2019; 2: 146–155.
33. Camanho P.P., Davila C.G., de Moura M.F. Numerical simulation of mixed-mode progressive delamination in composite materials. Journal of Composite Materials 2003; 37: 1415–1438.
34. Song K., Davila C., Rose C. Guidelines and parameter selection for the simulation of progressive delamination, in: ABAQUS User's Conf., 2008; 1–15.
35. Moslemi M., Khoshravan M. Cohesive zone parameters selection for mode-I prediction of interfacial delamination, Strojniški Vestnik – Journal of Mechanical Engineering 2015; 61: 507–516.
36. Lepore M.A., Perrella M. From test data to FE code: a straightforward strategy for modelling the structural bonding interface, Frattura Ed Integrità Strutturale 2016; 11: 191–201.
37. de Moura M.F.S.F., Campilho R.D.S.G., Gonçalves J.P.M. Pure mode II fracture characterization of composite bonded joints. International Journal of Solids and Structures, 2009; 46: 1589–1595.
38. Stuparu F.A., Constantinescu D.M. Interface damage characterization through cohesive parameters. Journal of Engineering Studies and Research 2012; 18: 129–139.
39. Mohammadi B., Salimi-Majd D. Investigation of delamination and damage due to free edge effects in composite laminates using cohesive interface elements. Engineering Solid Mechanics, 2014; 2: 101–118.
40. Soroush M., Fard K.M., Shahravi M. Finite element simulation of interlaminar and intralaminar damage in laminated composite plates subjected to impact. Latin American Journal of Solids and Structures 2018; 15.
41. Sitnikova E., Li D., Wei J., Yi X., Li S. On the representativeness of the cohesive zone model in the simulation of the delamination problem. Journal of Composites Science, 2019; 22.
42. Turon A., Dávila C.G., Camanho P.P., Costa J. An engineering solution for mesh size effects in the simulation of delamination using cohesive zone models. Engineering Fracture Mechanics 2007; 74: 1665–1682.
43. Alfano G., Crisfield M.A. Finite element interface models for the delamination analysis of laminated composites: mechanical and computational issues. International Journal for Numerical Methods in Engineering 2001; 50: 1701–1736.
44. Falk M.L., Needleman A., Rice J.R. A critical evaluation of dynamic fracture simulations using cohesive surfaces. J. Phys. IV Proc. 2001: 43–50.
45. Davila C., Camanho P., de Moura M. Mixed-mode decohesion elements for analyses of progressive delamination, in: 42nd AIAA/ASME/ASCE/AHS/ASC Struct. Struct. Dyn. Mater. Conf. 2001; 1–12.
46. Simulia ABAQUS 2019 User's Guide, 2019.
47. Wu E.M., Reuter R.C. Crack extension in fiberglass reinforced plastics, 1965.
48. Benzeggagh M.L., Kenane M. Measurement of mixed-mode delamination fracture toughness of unidirectional glass/epoxy composites with mixed-mode bending apparatus. Composites Science and Technology 1996; 56: 439–449.
49. Panettieri E., Fanteria D., Firrincieli A. Damage initialization techniques for non-sequential FE propagation analysis of delaminations in composite aerospace structures. Meccanica 2015; 50: 2569–2585.

50. Abdulla K.F., Cunningham L.S., Gillie M. Simulating masonry wall behaviour using a simplified micro-model approach, Engineering Structures 2017; 151: 349–365.
51. Zoghbi B.E. Modelling of failure mechanism in unidirectional carbon fiber-reinforced polyamide composites using cohesive zone model. International Journal of Composite Materials 2019; 9: 16–23,
52. Demir A., Ozturk H., Edip K., Stojmanovska M., Bogdanovic A. Effect of viscosity parameter on the numerical simulation of reinforced concrete deep beam behavior. The Online Journal of Science and Technology 2018; 8: 50–56.
53. Vu-Quoc L., Tan X.G. Optimal solid shells for non-linear analyses of multilayer composites. I. Statics, Computer Methods in Applied Mechanics and Engineering 2003; 192: 975–1016.
54. Tsai M.Y., Oplinger D.W., Morton J. Improved theoretical solutions for adhesive lap joints. International Journal of Solids and Structures 1998; 35: 1163–1185.
55. Tsai M.Y., Morton J. An investigation into the stresses in double-lap adhesive joints with laminated composite adherends. International Journal of Solids and Structures 2010; 47: 3317–3325.
56. Xiao X., Foss P.H., Schroeder J.A. Stiffness prediction of the double lap shear joint. Part1: Analytical solution. International Journal of Adhesion and Adhesives 2004; 24: 229–237.
57. Kläusler O., Clauß S., Lübke L., Trachsel J., Niemz P. Influence of moisture on stress–strain behaviour of adhesives used for structural bonding of wood. International Journal of Adhesion and Adhesives 2013; 44: 57–65.
58. Clauß S., Gabriel J., Karbach A., Matner M., Niemz P. Influence of the adhesive formulation on the mechanical properties and bonding performance of polyurethane prepolymers. Holzforschung 2011; 65: 835–844.
59. Hillerborg A., Modéer M., Petersson P.-E. Analysis of crack formation and crack growth in concrete by means of fracture mechanics and finite elements. Cement and Concrete Research 1976; 6: 773–781.